Identification of Coherent Structure in Turbulent Shear Flow With Wavelet Correlation Analysis

Hui Li
Department of Mechanical Engineering,
Faculty of Engineering,
Kagoshima University,
1-21-40, Korimoto,
Kagoshima City, Japan
Mem. ASME

In order to identify coherent structure of turbulent shear flow, a new combination of familiar techniques of signal processing, called wavelet correlation analysis, is developed based on the wavelet transform. The wavelet correlation analysis provides the unique capability for decomposing the correlation of arbitrary signals over a two-dimensional time delay-period plane. By analyzing two superposition functions implicating several pure frequencies, the correlation of periodic oscillations at several frequencies can well be separated and observed clearly. Coherent structures in the intermediate region of a plane turbulent jet are investigated using the wavelet correlation method. It is shown that the wavelet correlation analysis can extract the most essential scales governing features of eddy motions. The coherent structure information and apparent flapping behaviors are clearly revealed over a two-dimensional time-period plane.

Introduction

The topic of wavelet analysis is both very old and very new, because its roots can be traced back at least a century to the work of Weierstrass (1895), who described a family of functions that are constructed by superimposing scaled copies of a given base function. Another important early milestone was Haar's (1910) construction of the first orthonormal system of compactly supported functions, now called the Haar basis. As a tool for analysis of multiscale signals, the concept of wavelet transforms was first formalized in early 1980s by Morlet and Grossmann for the analysis of seismic data (Morlet et al., 1982; Goupillaud et al., 1984). They also outlined the mathematical foundations of the wavelets in 1984 (Grossmann and Morlet, 1984). Since then wavelets have been developed extensively by mathematicians and others. Over the last 15 years, exciting new developments in wavelet theory have attracted much attention and sparked new research in many fields, including pure and applied mathematics, physics, computer science, medicine, biology, and engineering. Few subjects have attracted scientists and engineers in other discipline as much attention as wavelets. New tools are available for efficient data compression, image analysis, and signal processing, and there is a great deal of activity in developing wavelet methods for use in these fields. The same features that make wavelets useful in these (and other) fields also make wavelets a natural and attractive choice to use in many areas of statistical data analysis.

The application of the wavelet analysis in the field of fluid mechanics started in 1988. Farge (1992, 1996) has given recent summaries of applications of wavelet analysis in the area of fluid mechanics. Numerous papers on this topic have been published rapidly, but from the view of fluids engineering these researchers can be broadly split into two categories. (1) Extracting the characters of turbulent or eddy structure from the wavelet analysis of experimental data and simulation data, and (2) developing turbulence modeling and numerical methods based on wavelet bases. In this study, we focus on the wavelet analysis of experimental data. In 1989 Argoul et al. used the wavelet transform to analyze the wind-tunnel turbulence data and provided the visual evidence of the celebrated Richardson cascade. From then the wavelet transform was widely used to reveal various turbulent or eddy structure, such as in fully developed turbulence (Yamada and Ohkitani, 1990; Bacry et al., 1991; Benzi and Vergassola, 1991), jets (Everson et al., 1990; Lewalle et al., 1994; Gordeyev et al., 1995; Gordeyev and Thomas, 1995; Li and Nozaki, 1995; Walker et al., 1995; Li, 1997a–d; Li et al., 1998a–c), boundary layers (Liandrat and Moret-Bailly, 1990; Benaissa et al., 1993; Kaspersen, 1996), bounded jets (Li et al., 1997), wall jets (Sullivan and Pollard, 1996), mixing layers (Dallard and Browand, 1993; Dallard and Spedding 1993), wake flows (Higuchi et al., 1994), surface wave fields (Spedding et al., 1993), multiphase flows (Li and Tomita, 1997, 1998), and others. Now, the wavelet transform has become a standard tool or software kit in identification of flow structure. Several new diagnostics (Farge, 1992; Li, 1997c) developed from the wavelet transform were employed to analyze structure of turbulence and eddy analysis. They offer the potential of extracting the essence of structure feature from flow fields, which are lost if using traditional statistics methods.

The aim of this paper is to apply the wavelets to analyzing the coherent structures in the near field of a turbulent plane jet. Since the coherent structure of a turbulent jet was first studied by Crow and Champagne (1971), the physics of a plane turbulent jet has been widely investigated for several decades (Gutmark, 1976; Moum et al., 1979; Goldschmidt et al., 1981; Gervantes and Goldschmidt, 1981; Krothapalli et al., 1981; Weir et al., 1981; Mumford, 1982; Antonia et al., 1983; Oler et al., 1984; Yoda et al., 1992; Tomas and Chu, 1993; Quinn, 1994; Hsiao and Huang, 1994). It has become a well-known fact that the large-scale eddy motion of the plane turbulent jet exhibits a symmetric, periodic and apparent flapping motion in similarity region. Coherent structures are known to exist and be responsible for most of the momentum transfer in plane turbulent jets. Furthermore, many identification techniques, such as visualization, spectra analysis, spatial correlation functions, education schemes, proper orthogonal decomposition, stochastic estimation, pattern recognition, and wavelet transform, are well established to determine coherent structures. However, the local pe-

Contributed by the Fluids Engineering Division for publication in the JOURNAL OF FLUIDS ENGINEERING. Manuscript received by the Fluids Engineering Division November 22, 1996; revised manuscript received June 9, 1998. Associate Technical Editor: F. Giralt.

riod with respect to space-time changes continuously for the turbulence and large-scale eddy motion, and the coherent structure in both time and period spaces has not yet been clarified. Identification of coherent structure requires the acquisition of detailed quantitative data on such structure characteristics as size, strength, convection velocity, etc. Neither the Fourier analysis nor the traditional correlation method gives us sufficient information. To solve these problems two methods, (1) more powerful identification techniques and (2) simultaneous multipoints or full field measurements, must be considered. In present study we focus on the development of the new identification technique.

The major motivation of this paper is to develop a new correlation method based on the wavelet transform, referred to as the wavelet correlation analysis. This approach can overcome limitations of the traditional correlation method which only describes the correlation of signals in terms of time delay, and assist analysis of the similarity structure of signals in terms of scale and time delay. The traditional correlation method still plays an important role, but it had been hiding the essence of the similarity feature since it lacks frequency resolution. Then the experimental fluctuating velocities at various spatial locations in the near field of a plane turbulent jet are analyzed by the wavelet correlation analysis to reveal coherent structures over a two-dimensional time-period plane, and to extract the most essential scales governing the features of eddy motions.

Definition of Continuous Wavelet Transform

The continuous wavelet transform of a real square integrable function $f(t) \in L^2(\Re)$ (where $L^2(\Re)$ denotes the Hilbert space of measure) at a location b, relative to a real integrable analyzing wavelet $\psi(t)$ at scale a, can be defined as

$$Wf(b, a) = \frac{1}{a}\int_{-\infty}^{\infty} f(t)\,\overline{\psi\left(\frac{t-b}{a}\right)}\,dt. \qquad (1a)$$

Equivalently,

$$Wf(b, a) = \langle f, \psi_{b,a}\rangle, \qquad (1b)$$

where $Wf(b, a)$ is called the wavelet coefficient, $^-$ stands for complex conjugate and

$$\psi_{b,a} = \frac{1}{a}\,\overline{\psi\left(\frac{t-b}{a}\right)}\,.$$

It can be seen that $\psi_{b,a}$ plays the same role as $e^{i\omega t}$ in the definition of the Fourier transform. The continuous wavelet transform is commonly viewed as a numerical microscope whose optics, magnification, and position are given by $\psi(t)$, a, and b, respectively.

In Fourier space the wavelet transform can be expressed as

$$Wf(b, a) = \frac{1}{2\pi}\int_{-\infty}^{\infty} \hat{f}(\omega)\overline{\hat{\psi}_{b,a}(\omega)}\,e^{ib\omega}d\omega, \qquad (2)$$

where $\hat{f}$ and $\hat{\psi}$ are the Fourier transforms of f and ψ, respectively.

In order to understand the time-frequency localization properties of wavelet transforms, we need to study the behaviors of the standard deviation of $|\psi_{b,a}(t)|^2$ and $|\hat{\psi}_{b,a}(\omega)|^2$, i.e., $\sigma_{\psi_{b,a}}$ and $\sigma_{\hat{\psi}_{b,a}}$. It is easy to verify the following relationships:

$$\sigma_{\psi_{b,a}} = \sqrt{a}\,\sigma_{\psi_{0,1}} \quad \text{and} \quad \sigma_{\hat{\psi}_{b,a}} = \frac{\sigma_{\hat{\psi}_{0,1}}}{a^{2/3}}\,. \qquad (3)$$

From the above relationships it can be easily seen that $\sigma_{\psi_{b,a}}$ increases and $\sigma_{\hat{\psi}_{b,a}}$ decreases with increasing the scale a, and vice-versa. This indicates that wavelet transform can detect high frequency components of signals with sharper time resolution and low frequency components of signals with sharper frequency resolution. This advantage overcomes the limitations of using a fixing scale of window in the short-time Fourier transform.

An arbitrary function satisfying the admissibility condition of wavelet may be used as an analyzing wavelet. Several well-defined wavelet functions, such as Haar, Paul, French hat, *m*-th derivatives of the Gaussian, Mexican hat, Morlet and Gabor wavelet, are commonly used as the analyzing wavelet. The choice of the appropriate wavelet function is at the user's disposal and depends on the kind of information that we want to extract from the signal. In this paper we adopt the continuous wavelet transform and the Morlet wavelet function (a complex-valued function), which often appeared in fluid mechanics. The Morlet wavelet function is given by

$$\psi(t) = \pi^{-1/4}e^{-i\omega_0 t}\,e^{-t^2/2}. \qquad (4a)$$

which satisfies $\|\psi\|^2 = 1$, and its Fourier transform is written as

$$\hat{\psi}(\omega) = \sqrt{2}\,\pi^{1/4}e^{-(\omega-\omega_0)^2/2}. \qquad (4b)$$

It is obvious that the Morlet wavelet function $\psi(t)$ is localized around $t = 0$, and $\hat{\psi}(\omega)$ is localized around the central of passing band $\omega_c = \omega_0$. In practical applications of signal processing it has been found that a particularly useful value for ω_c is the one for which the wavelet scale a represents the period. Therefore, the central of passing band is defined as $\omega_c = \omega_0 = 2\pi$ in this paper. Then $\psi_{b,a}(t)$ is centered at the position b with the standard deviation $\sqrt{a/2}$, and $\hat{\psi}_{b,a}(\omega)$ is centered at the central of passing band $2\pi/a$ with the standard deviation $\sqrt{\pi/2a^3}$. This wavelet function is complex, enabling one to extract information about amplitude and phase of the process being analyzed. Using the Morlet wavelet function, wavelet coefficients of Eq. (1) can describe a signal as localized strength of a signal over a two-dimensional time-period plane.

Wavelet Auto-Correlation Function

In any nonstationary situation, such as in human speech, music, velocity signals of turbulence and others, signals contain various frequency components that rapidly change with time in complex ways. The traditional auto-correlation method is quite capable in identifying the self-similarity structure. However, it cannot extract the information of the self-similarity structure in frequency space and had been hiding the essence of the self-similarity feature since it lacks frequency resolution. The traditional auto-correlation method is well suited to analyze the periodic signals and is not suited for complex signal analysis. Although the wavelet transform can describe *when* those frequency components occurred, more powerful techniques must be developed to gain deeper insight into the complex self-similarity behavior of signals.

As described in the previous section, wavelet coefficients can describe a signal as localized strength of the signal in both time and period or frequency spaces. The modulus, real part, and phase of wavelet coefficients have been employing to describe the characteristics of a signal. Therefore the all traditional statistics method may be applied. In order to obtain the self-similarity structure of a signal for various scales at any given time delay, at first, we unfold the signal into a two-dimensional time-period plane by the wavelet transform. Then we use its wavelet coefficients to define an auto-correlation function, called the *wavelet auto-correlation function* $WC(a, \tau)$, by the following formula.

$$WC(a, \tau) = \lim_{T\to\infty}\frac{1}{T}\int_{-2/T}^{2/T}\overline{Wf(b, a)}\,Wf(b+\tau, a)db, \quad (5)$$

where τ is time delay of wavelet coefficients in the wavelet space, or the time delay of the signal $f(t)$. It is evident that the wavelet auto-correlation function can provide important self-

similarity features on a two-dimensional period-time delay plane, and then extracts the most essential frequencies governing the self-similarity features of signals.

The wavelet auto-correlation function $WC(a, \tau)$ can also be written in Fourier space

$$WC(a, \tau) = \frac{1}{2\pi}\int_{-\infty}^{\infty} S(\omega)|\hat{\psi}(a\omega)|^2 e^{i\tau\omega}d\omega. \quad (6)$$

Equation (6) is very similar to the wavelet transform of Eq. (2) in either form or the physical sense. Equation (6) represents the relationship between wavelet space and Fourier space, and demonstrates the characteristic of $WC(a, \tau)$ as a local filter, in which the Fourier power spectrum $S(\omega)$ is filtered by $|\hat{\psi}(a\omega)|^2$ in Fourier space.

We define a local wavelet power spectrum density function $WP(a, \omega)$ as follows

$$WP(a, \omega) = S(\omega)|\hat{\psi}(a\omega)|^2. \quad (7)$$

Substituting Eq. (7) into Eq. (6), we obtain

$$WC(a, \tau) = \frac{1}{2\pi}\int_{-\infty}^{\infty} WP(a, \omega)e^{i\tau\omega}d\omega. \quad (8)$$

With the inverse Fourier transform the above equation becomes

$$WP(a, \omega) = \int_{-\infty}^{\infty} WC(a, \tau)e^{-i\tau\omega}d\tau. \quad (9)$$

From Eq. (8) and (9) it is obvious that $WP(a, \omega)$ may be defined as the Fourier transform of $WC(a, \tau)$, and $WC(a, \tau)$ may be obtained from the inverse Fourier transform of $WP(a, \omega)$. This relationship is same as the Wiener-Khintchine theorem of the traditional auto-correlation.

If a complex-valued function is used as the analyzing wavelet, the wavelet coefficient becomes a complex-valued function. Hence $WC(a, \tau)$ is also a complex-valued function from the definition of the wavelet auto-correlation function in Eq. (5) or (6). In order to extract information of the self-similarity structure of signals, the modulus $MWC(a, \tau)$ and the phase $\theta WC(a, \tau)$ of wavelet auto-correlation function are employed to express the strength of auto-correlation and the average phase difference for different time delay of signals at a given period, respectively. The real part of wavelet auto-correlation function $RWC(a, \tau)$ is used to reveal the information of positive and negative correlation.

In this paper, we define a wavelet auto-correlation coefficient $RWR(a, \tau)$, which is normalized with respect to the wavelet auto-correlation function at $\tau = 0$ or the wavelet power spectrum density function $RWC(a, 0)$, as follows:

$$RWR(a, \tau) = \frac{RWC(a, \tau)}{RWC(a, 0)}, \quad (10)$$

where $RWR(a, 0) = 1$ and $|RWR(a, \tau)| \leq 1$.

Wavelet Cross-Correlation Function

In identifying the spatial turbulent structure or coherent structures and its evolution in time, the cross-correlation analysis between velocity components measured at two separated points in flow filed is most used. A difficulty with the traditional cross-correlation method, however, is that the cross-correlation function only provides information about the cross-correlation behavior in terms of time delay but no information about correlation behaviors in scale space at each scale due to lack of scale resolution.

In analogy with the wavelet auto-correlation, we first unfold, respectively, two different signals $f_x(t)$ and $f_y(t)$ into their two-dimensional time-period planes using the wavelet transform, in order to yield the period resolution. Then their wavelet coefficients, $Wf_x(b, a)$ and $Wf_y(b, a)$, are used to define a cross-correlation function, called the *wavelet cross-correlation function* $WC_{xy}(a, \tau)$, by the following formula.

$$WC_{xy}(a, \tau) = \lim_{T\to\infty}\frac{1}{T}\int_{-2/T}^{2/T} \overline{Wf_x(b, a)}Wf_y(b + \tau, a)db, \quad (11)$$

where τ is a time delay between two signals. The wavelet cross-correlation function has the following two characteristics. (1) Since the wavelet cross-correlation function is obtained by integration of wavelet coefficients over time plane, contributions of different period to the correlation are kept reasonably separated. (2) This separation is achieved without excessive loss of resolution in time variable due to use of the wavelet transform (of course, subject to the limitation of the uncertainty principle). The two characteristics exhibit the property known as time-period localization. Therefore, the wavelet cross-correlation function can describe important statistical correlation features between two different signals on a two-dimensional scale-time delay plane, and extract the most essential scales governing the correlation features, which is lost if using traditional method.

In Fourier space, the wavelet cross-correlation function $WC_{xy}(a, \tau)$ can also be written as

$$WC_{xy}(a, \tau) = \frac{1}{2\pi}\int_{-\infty}^{\infty} S_{xy}(\omega)|\hat{\psi}(a\omega)|^2 e^{i\tau\omega}d\omega, \quad (12)$$

where $S_{xy}(\omega)$ is the traditional cross-spectrum. Expression (12) represents the relationship between the wavelet and Fourier spaces, and describes the characteristic of $WC_{xy}(a, \tau)$ as a local filter, in which the Fourier power spectrum $S_{xy}(\omega)$ is filtered by $|\hat{\psi}(a\omega)|^2$ in Fourier space. Here we define a local wavelet cross-spectrum function $WP_{xy}(a, \omega)$ as

$$WP_{xy}(a, \omega) = S_{xy}(\omega)|\hat{\psi}(a\omega)|^2. \quad (13)$$

Substituting Eq. (13) into Eq. (12), we obtain

$$WC_{xy}(a, \tau) = \frac{1}{2\pi}\int_{-\infty}^{\infty} WP_{xy}(a, \omega)e^{i\tau\omega}d\omega. \quad (14)$$

Carrying out an inverse Fourier transform the above equation becomes

$$WP_{xy}(a, \omega) = \int_{-\infty}^{\infty} WC_{xy}(a, \tau)e^{-i\tau\omega}d\tau. \quad (15)$$

From Eqs. (14) and (15), $WP_{xy}(a, \omega)$ can be defined as the Fourier transform of $WC_{xy}(a, \tau)$, and $WC_{xy}(a, \tau)$ can be obtained from the inverse Fourier transform of $WP_{xy}(a, \omega)$. This relationship is very similar to the Wiener-Khintchine theorem of the traditional cross-correlation.

In order to characterize the cross-correlation, we may use a modulus of wavelet cross-correlation coefficients $MWR_{xy}(a, \tau)$ and a phase of wavelet cross-correlation function $\theta WC_{xy}(a, \tau)$ to describe the strength of cross-correlation and the average phase difference between two signals in terms of time delay and period. However, $MWR_{xy}(a, \tau)$ can not provide an information of negative cross-correlation. Therefore, it is convenient to introduce a real part of wavelet cross-correlation coefficients $RWR_{xy}(a, \tau)$ by

$$RWR_{xy}(a, \tau) = \frac{RWC_{xy}(a, \tau)}{\sqrt{RWC_x(a, 0)RWC_y(a, 0)}}. \quad (16)$$

where $RWC_x(a, 0)$ and $RWC_y(a, 0)$ are the real parts of wavelet auto-correlation functions at $\tau = 0$.

Wavelet Correlation Analysis of Superposition Functions

First, the following function, which is a superposition of n pure frequencies at frequencies $\omega_1, \omega_2 \ldots \omega_n$,

$$f(t) = \sum_{k=1}^{n} \mathrm{Exp}(i\omega_k t). \quad (17)$$

is analyzed by the wavelet transform.

Clearly, the superposition principle tells us the wavelet transform of a superposition function is the superposition of the respective transforms. Using Eq. (1) the wavelet transform of function (17) can be written as

$$Wf(b, a) = \sum_{k=1}^{n} \exp(i\omega_k b)\overline{\hat{\psi}(a\omega_k)}. \quad (18)$$

If $\hat{\psi}(\omega)$ has zero imaginary part, the real part and imaginary part of wavelet coefficient correspond to the wavelet transform of the real part and imaginary part of the superposition function, respectively.

Consider the following two superposition functions,

$$f_x(t) = \sum_{j=1}^{n} \mathrm{Exp}(i\omega_j t) \quad \text{and} \quad f_y(t) = \sum_{k=1}^{n} \mathrm{Exp}(i\omega_k t). \quad (19)$$

Using Eq. (12) the wavelet cross-correlation solution of the above two functions (Eq. (19)) can be obtained as

$$WC_{xy}(a, \tau) = \sum_{j=1}^{n}\sum_{k=1}^{n} \hat{\psi}(a\omega_j)\overline{\hat{\psi}(a\omega_k)}\,\mathrm{Exp}(i\omega_j\tau) \lim_{T\to\infty} \frac{1}{T}\int_{-T/2}^{T/2} \times \mathrm{Exp}(i(\omega_j - \omega_k)b)db. \quad (20a)$$

From the above equation, the analyzing solution of the wavelet cross-correlation function can be written as the following formula.

(1) If $\omega_j \neq \omega_k$, then $\lim_{T\to\infty} \frac{1}{T}\int_{-T/2}^{T/2} \mathrm{Exp}(i(\omega_j - \omega_k)b)db = 0$,

Thus $WC_{xy}(a, \tau) = 0$.

(2) If $\omega_j = \omega_k$, then $\lim_{T\to\infty} \frac{1}{T}\int_{-T/2}^{T/2} \mathrm{Exp}(i(\omega_j - \omega_k)b)db = 1$,

Thus $WC_{xy}(a, \tau)$

$$= \sum_{j=1}^{n}\sum_{k=1}^{n} \hat{\psi}(a\omega_j)\overline{\hat{\psi}(a\omega_k)}\,\mathrm{Exp}(i\omega_j\tau). \quad (20b)$$

From the above relationships, it is obvious that the real part of wavelet cross-correlation function (Eq. (20*b*)) gives the cross-correlation between the real parts of two superposition functions.

Consider, for example, two different functions contain the superposition of three pure frequencies ($n = 3$) at frequencies $\omega_1 = \pi/4$, $\omega_2 = \pi/2$, $\omega_3 = \pi$ and $\omega_1 = \pi/4$, $\omega_2 = \pi/2$, $\omega_3 = 2\pi$, respectively. It is evident that two functions have common frequencies at $\pi/4$ and $\pi/2$. Using Eq. (21), the real part of the wavelet cross-correlation function $RWC_{xy}(a, \tau)$ is calculated with the help of the Morlet wavelet function, and is shown on the (a, τ) plane representation in Fig. 1. From the distributions of $RWC_{xy}(a, \tau)$, we can obtain the cross-correlation at various periods and time delay.

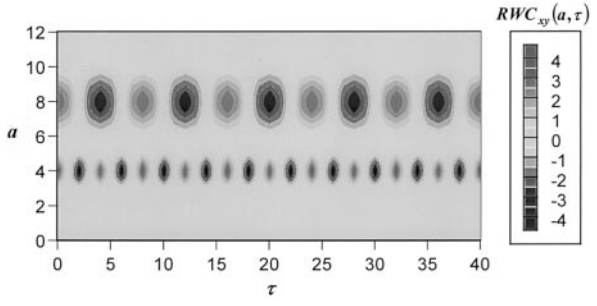

Fig. 1 Wavelet cross-correlation analysis of two superposition functions

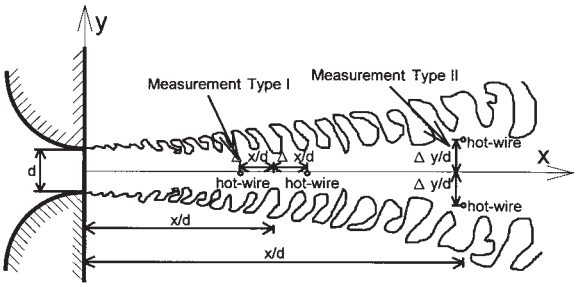

Fig. 2 Sketch of the experimental configuration

Two groups of periodic peaks at $a = 4(\omega = \pi/2)$ and $8(\omega = \pi/4)$ can clearly be observed, and the strong periodic correlation at the two frequencies are well detected. However, two groups of periodic oscillations at $\omega = \pi$ and 2π, which exist respectively in two wavelet coefficients (or functions), are destroyed. This indicates no correlation at the two frequencies.

Experimental Apparatus and Procedure

A definition sketch of a plane jet is shown in Fig. 2, where x is the streamwise coordinate and y is the lateral coordinate. The jet was generated by a blower-type wind tunnel with flow-straightening elements, screens, settling length and a 24:1 contraction leading to a 350 mm × 25 mm nozzle. The nozzle width d is 25 mm and the aspect ratio of nozzle is 14. The measurements were performed at a Reynolds number (based upon exit mean velocity, U_a, and nozzle width, d) of Re = 3330 which corresponded to an exit velocity of $U_a = 2$ m/s. The measured exit turbulent intensity on the jet centerline is less than 0.04%. The velocity of the x-component was measured simultaneously using two standard hot wire probes located in the (x, y)-plane. In the present experiment, as shown in Fig. 2, the following two type measurements were carried out. (1) Type I measurements were performed with two probes for equal separations distances Δx centered at x on the jet centerline; and (2) type II measurements were performed with two probes at equal separate distances Δy from the jet centerline at various x locations. For the measurements with streamwise separation (type I), the present minimum value of $2\Delta x$ (= 25 mm) was such that the thermal wakes from the upstream hot wire did not interfere with the downstream probe. The statistics of velocity obtained from the downstream probe were unaffected by the presence of the upstream probe. The recording frequency of data is 2 kHz, and the recording length is 4 seconds.

The measurement errors due to the sensitivity of hot wire probe were the most dominant, other errors can be negligible. The uncertainty at 95 percent confidence for the wavelet correlation coefficient and its phase are approximately about 10 percent.

Application to a Plane Turbulent Jet

Wavelet Auto-Correlation Analysis of Flow Structure. In order to investigate self-similarity structures of the jet at various periods, the wavelet auto-correlation of the x-component of fluctuating velocities on the centerline at $x/d = 8.5$ are first analyzed. The modulus of the wavelet auto-correlation function $MWC(a, \tau)$ with its real part $RWC(a, \tau)$ is shown on the (a, τ) color plane (abscissa: time delay τ, ordinate: period a, rainbow colors for wavelet auto-correlation magnitudes) in Fig. 3. Below these color plates, the traditional auto-correlation coefficients $R(\tau)$ are also illustrated.

It is evident that $RWC(a, \tau)$ shows almost same distribution as $MWC(a, \tau)$. $RWC(a, \tau)$ not only gives exactly same the

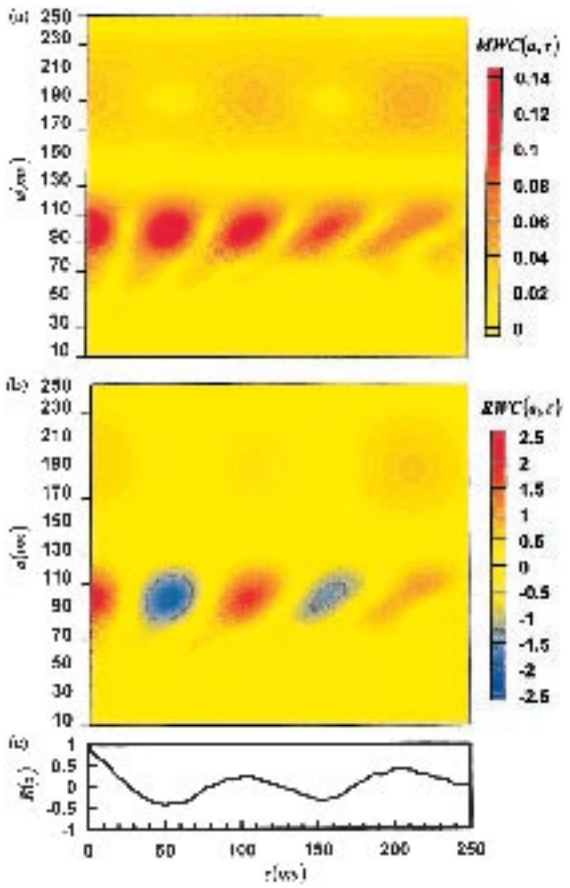

Fig. 3 Wavelet auto-correlation analysis of fluctuating velocity on the centerline at $x/d = 8.5$; (*a*) modulus of wavelet auto-correlation function; (*b*) real part of wavelet auto-correlation function; (*c*) traditional auto-correlation coefficients

information as $MWC(a, \tau)$, but also extracts local positive and negative correlation within the period a centered at τ. Therefore, it is proper that $RWC(a, \tau)$ replaces $MWC(a, \tau)$ to express the strength of the wavelet auto-correlation. In the following section, we utilize $RWC(a, \tau)$ to analyze the flow structure instead of $MWC(a, \tau)$. From the distribution of $RWC(a, \tau)$ in Fig. 3(a), the dominant distributions of two periodic oscillations at $a = 100$ and 195 ms are evident, and indicate that the periodic motions with two scales through the centerline. Making a comparison between $RWC(a, \tau)$ and $R(\tau)$, we find that the large positive and negative peaks in $R(\tau)$ correspond to the alternative strong positive and negative peaks of $RWC(a, \tau)$ at $a = 100-110$ ms. However, from $R(\tau)$ peaks and the information on auto-correlation appearing at $RWC(a, \tau)$ of $a = 195$ ms cannot be found. It is because its magnitude is smaller than that of $a = 100-110$ ms, and its effects are embedded due to the presence of the other scale. Although power spectrum may clearly describe peaks of auto-correlation in frequency space, it is impossible to provide information on the strength of auto-correlation responding to the changing the time delay.

Then, $RWR(a, \tau)$ and $\theta WC(a, \tau)$ for the x-component of the fluctuating velocity in the shear layer at $x/d = 10$ and $y/d = 2.5$ are shown in Fig. 4. $RWR(a, \tau)$ obviously gives a maximum (equal to the wavelet power spectrum density) at $\tau = 0$, i.e., $RWR(a, 0) = 1$. The traditional auto-correlation decreases to zero as τ increases, and does not provide any information of self-similar flow structure. However, From $RWR(a, \tau)$ the obvious periodic oscillations happen at $a = 15$, 40, 75, 100 and 150 ms, and imply strong periodic motions passing the shear layer. Among these periodic multi-scale motions, the stronger coherence appear at $a = 75$, 100 and 150 ms. The distribution of $RWR(a, \tau)$ also shows a map of apparent multi-scale similarity structure in the shear layer. From a positive peak at $a = 150$ ms, a large branching structure, which consists of two peaks at $a = 100$ ms, may be clearly observed around $\tau = 170$ ms. This indicates that a complex periodic larger-scale motion (or large eddy structure), which contains periodic smaller-scale motions (or small eddies), exists in the shear layer.

The values of $RWR(a, \tau)$ are larger than that of $R(\tau)$, because the traditional auto-correlation is the results of interference among auto-correlation magnitudes of all periods at a given time delay. Making a comparison between $RWR(a, \tau)$ and $R(\tau)$ it is found that the interference between the positive and negative magnitudes at various periods around τ may produce the zero value of $R(\tau)$. However, there must be existence of correlation at some period, and this means that $R(\tau)$ may hide some important coherent information. But the wavelet auto-correlation analysis can extract all information existing in the complex flow structure.

On the other hand, $\theta WC(a, \tau)$ expresses the distribution of phase difference between $\tau = 0$ and τ at any given period. The discontinue constant phase lines and the range of zero value in $\theta WC(a, \tau)$ correspond to the zero real part of auto-correlation lines and the region of the positive or negative peak in the map of $RWR(a, \tau)$, respectively. The cross-point of constant-phase lines equivalents to zero point of $MWC(a, \tau)$ which means noncorrelation. The distribution of the cross-point along the discontinue constant-phase lines decreases rapidly as the period increases, and this indicates that the periodic flow structure consists of many small-scale motions and few large-scale motion. From the distribution of the wavelet phase difference $\theta WC(a, \tau)$ between $\tau = 0$ and τ in Fig. 4(b), it is evident

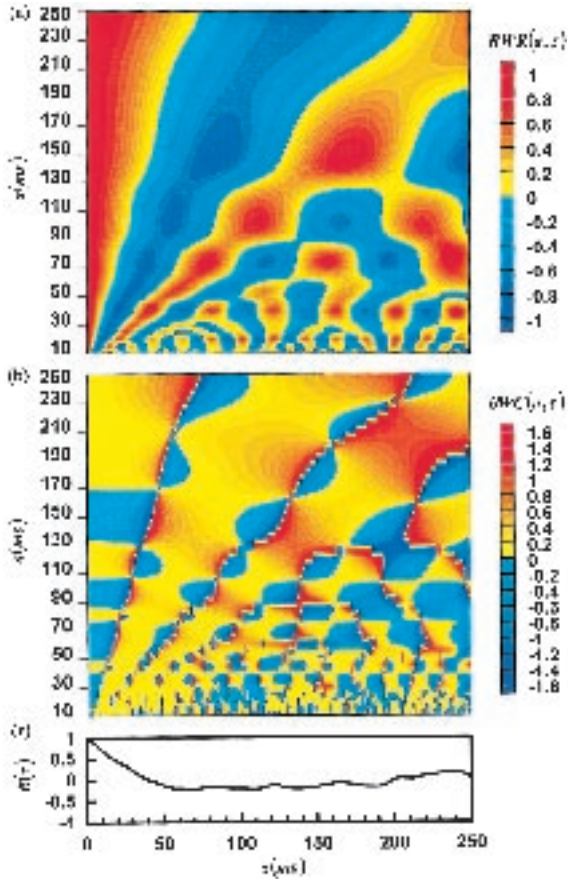

Fig. 4 Wavelet auto-correlation analysis of fluctuating velocity in the shear layer at $x/d = 10$ and $y/d = 2.5$; (*a*) wavelet auto-correlation coefficients; (*b*) phase of wavelet auto-correlation function; (*c*) traditional auto-correlation coefficients

that the interval of the discontinue constant-phase lines increases with the period. At any given period or scale, we can obtain an angular frequency $\omega(a, \tau)$ $(=\Delta\theta WC(a, \tau)/\Delta\tau)$ by differentiating the corresponding phase fields with respect to τ. In fact, $\omega(a, \tau)$ means the difference of the angular frequency between $\tau = 0$ and τ.

Wavelet Cross-Correlation Analysis of Coherent Structure (Type I Measurement). For identifying the organized structure in the turbulent plane jet, the wavelet cross-correlation coefficients $RWR_{xy}(a, \tau)$ and its phase $\theta WC_{xy}(a, \tau)$ between two x-components of fluctuating velocities are calculated for $2\Delta x/d = 2$ separation distances on the centerline at x/d ratios of 5, and are shown in Fig. 5 (abscissa: time delay τ, ordinate: period a, rainbow colors: amplitude of $RWR_{xy}(a, \tau)$ or $\theta WC_{xy}(a, \tau)$). Below the color plates, the result of the traditional cross-correlation coefficients $R_{xy}(\tau)$ is also plotted.

Making a comparison between $RWR_{xy}(a, \tau)$ and $R_{xy}(\tau)$, the large peaks of $R_{xy}(\tau)$ correspond to the nearly periodic correlation peaks at $a = 80-105$ ms, and the small peaks of $R_{xy}(\tau)$ equivalent to the nearly periodic peaks of $RWR_{xy}(a, \tau)$ below $a = 50$ ms. From the distributions of $RWR_{xy}(a, \tau)$, the branching structures can clearly be observed as follows. A strong positive correlation peak in high period range ($a = 145$ ms) at $\tau = 185$ ms is composed of two positive correlation peaks of medium period ($a = 105$ ms) at $\tau = 130$ and 230 ms. Furthermore, each of correlation peaks in medium period range consists of two correlation peaks in low period range. This implies that the periodic large-scale motion (or periodic large eddy) contains that of smaller scale (or periodic small eddies). With increasing τ, as shown in Fig. 5(a), the alternative positive and negative

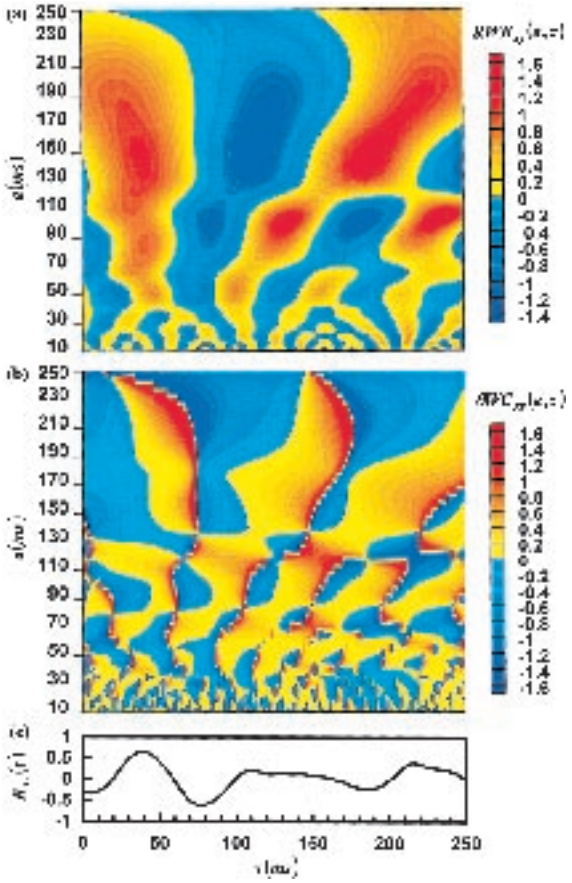

Fig. 5 Wavelet cross-correlation analysis of two velocity fluctuations at $x/d = 5$, $2\Delta x/d = 2$ (Type I); (a) wavelet cross-correlation coefficients; (b) phase of wavelet cross-correlation function; (c) traditional cross-correlation coefficients

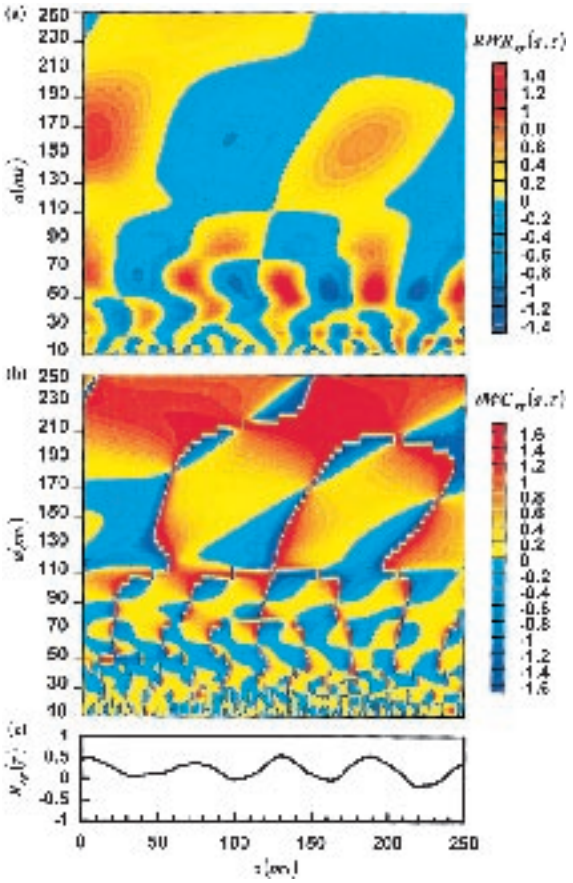

Fig. 6 Wavelet cross-correlation analysis of two velocity fluctuations at $x/d = 5$, $2\Delta y/d = 2$ (type II); (a) wavelet cross-correlation coefficients; (b) phase of wavelet cross-correlation function; (c) traditional cross-correlation coefficients

peaks at various periods are observed. The dominant feature of this figure is two periodic oscillation at $a = 145$ ms and at $a = 105$ ms after $\tau = 85$ ms, respectively. Four cycles of oscillations at $a = 50$ ms can also be observed. This indicates that the periodic eddies of $a = 50$, 105 and 145 ms pass through the shear layer, because the local potential core fluctuating ve-

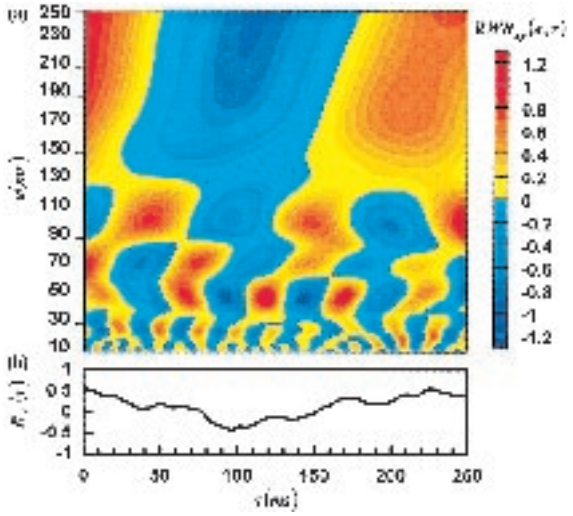

Fig. 7 Wavelet cross-correlation analysis of two velocity fluctuations at $x/d = 10$, $2\Delta y/d = 0.5$ (Type II) (a) wavelet cross-correlation coefficients; (b) traditional cross-correlation coefficients

locity has unusually large positive and negative peaks when an eddy moves close to the center line (Yule, 1978). There are weaker patterns in the range of $a = 20-30$ ms, and this indicates the existence of weaker periodic motions. The first positive peak of $R_{xy}(\tau)$ corresponds to two positive peaks of $RWR_{xy}(a, \tau)$ at $a = 85$ and 145 ms, which give the periods of eddy motion. Because $RWR_{xy}(a, \tau)$ has a strongly negative peak at period $a = 80$ ms at zero time delay, $R_{xy}(\tau)$ exhibits a negative value. However, this does not mean the negative correlation in all period range.

The second color graph of Fig. 5 shows a distribution of its $\theta WC_{xy}(a, \tau)$ using (a, τ) color plane representation. $\theta WC_{xy}(a, \tau)$ can describe the phase difference between two wavelet coefficients or two velocity fluctuations at two different locations for a time delay of τ at a given period a, and can help us identify the change of the phase difference from $-(\pi/2)$ to $\pi/2$. The discontinue isophase line between isophase line of $\pi/2$ and $-(\pi/2)$ corresponds to the zero value line of $RWR_{xy}(a, \tau)$, which means non-correlation. The zero isophase line of $\theta WC_{xy}(a, \tau)$ equivalents to the local maxima or minima of $RWR_{xy}(a, \tau)$ around τ at a given a, and this indicates that two signals at two points have a same phase value. Of course, positive or negative peaks in the map of $RWR_{xy}(a, \tau)$ exist on the zero isophase lines. A cross-point, which exists a cross between a zero isophase line and a discontinue isophase line, corresponds to the zero value of the modulus of wavelet cross-correlation coefficient $MWR_{xy}(a, \tau)$. The branching structures of the discontinue isophase line or the zero isophase line also indicate that the periodic flow structure consists of many periodic small-scale motions and few periodic large-scale motion. At a given period or scale, we can obtain an angular frequency $\omega_{xy}(a, \tau)$ $(=\Delta\theta WC_{xy}(a, \tau)/\Delta\tau)$ by differentiating the corresponding phase fields with respect to time delay. In fact, $\omega_{xy}(a, \tau)$ means the difference of the angular frequency between the two velocity fluctuations at two points for a time delay of τ.

It is well known that the traditional cross-correlation of velocity fluctuations has been used extensively to determine the convection velocity in various turbulent flows. Although Goldschmidt et al. (1981) considered both broadband and wavenumber-dependent convection velocities, and dominant convection velocities cannot be extracted. From the distribution of peaks in $RWR_{xy}(a, \tau)$, however, we can easily determine the convection velocities of various periods that dominate flow structures using the following method. The convection velocity for a given period is defined as the ratio of the longitudinal separation distance $2\Delta x$ between two probes and the time delay τ_{max} between local maxima or minima in $RWR_{xy}(a, \tau)$, or the ratio of the longitudinal separation distance $2\Delta x$ and the period a_{max} at which $RWR_{xy}(a, \tau)$ has the local maxima or minima. From the distribution of peaks in $RWR_{xy}(a, \tau)$ for various periods, it is obvious that the convection velocity is period dependent. The time delay between local maxima or local minima of $RWR_{xy}(a, \tau)$ clearly indicates that the large-scale motion moves slower than the small-scale motion.

Wavelet Cross-Correlation Analysis of Coherent Structure (Type II Measurement). Type II measurements were used to investigate the coherent structure of turbulent flow on opposite sides of the centerline in the shear layer. Color contour maps of $RWR_{xy}(a, \tau)$ and $\theta WC_{xy}(a, \tau)$ of the two fluctuating velocities with separations of $2\Delta y/d = 2$ at $x/d = 5$ in the shear layer are shown in Fig. 6. It exhibits positive values for $RWR_{xy}(a, \tau)$ at zero time delay and periodic oscillations for various periods with increasing the time delay. This indicates that symmetric and periodic motions with various scales exist in the shear layer. From Fig. 6(*a*), the obvious nearly periodic oscillations happen at $a = 65$, 90 ($\tau = 100-190$ ms), 160 ms, and several irregular weaker peaks at $a < 50$ ms range. This implies that the two-dimensionality of the periodic vortex street contains three periodic eddies and several irregular small eddies on opposite sides of the centerline. From the branching structures in $RWR_{xy}(a, \tau)$, the periodic eddy of $a = 90$ ms, which exists in the periodic large eddy of $a = 160$ ms, contains the periodic eddy of $a = 65$ ms. Above coherent structure is essentially coincident with what we find in Fig. 5. The distribution of $\theta WC_{xy}(a, \tau)$ is shown in Fig. 6(*b*). The cross-point and area of positive value of phase increase with increasing separation distance of $2\Delta y/d$. This implies that the periodic motions with various scales are much more active in the shear layer. The distribution of $\theta WC_{xy}(a, \tau)$ shows regular features in range of medium and high period, because periodic medium and large scale eddies appear in the shear layer. However, the distribution of $\theta WC_{xy}(a, \tau)$ becomes the most irregular features in low period range.

At a downstream distance of $x/d = 10$, the variation in $RWR_{xy}(a, \tau)$ for a separation of $2\Delta y/d = 0.5$ is shown in Fig. 7. It is apparent that the strong periodic correlation occurs at $a = 50$, 70, 105 ms, and high period range. There are also weaker periodic peaks appearing at $a < 30$ ms. Comparing with $RWR_{xy}(a, \tau)$ at $x/d = 5$ (Fig. 6(*a*)), the scale of dominant periodic eddy increases.

It is well-known fact that the turbulent plane jet exhibits an apparent sideways, flapping type motion (Goldschmidt and Bradshaw, 1973). The apparent flapping motion attributes either to the presence of organized coherent structures with lateral oscillations of finite extent or to an asymmetric coherent structure, which is hidden in the randomness of the turbulent field. This motion can be detected only by the distinctive negative correlation at zero time delay after long time averaged correlation of the longitudinal components of the velocity measured at two points, each one at opposite sides of the jet centerline (Gervantes and Goldschmidt, 1981). However, it is impossible to provide the information about the scale or period of this motion from the traditional correlation method. At $x/d = 10$, as shown in Fig. 7(*a*), the distinctive positive values appearing in $R_{xy}(\tau)$ at zero time delay. Usually this indicates the asymmetric organized motion and means no flapping motion at all. In this study we describe the flapping motion in the Fourier space using the wavelet cross-correlation analysis. From the distinctive positive values appearing in $RWR_{xy}(a, \tau)$ at zero time delay in Fig. 7(*a*), the symmetric organized structures can be detected at $a = 50$, 70 ms and high period range. However, $RWR_{xy}(a, \tau)$ at $a = 105$ ms and low period range exhibits the distinctive negative values at zero time delay. This implies that the apparent flapping behavior appears at these periods or scales, which is masked by the symmetric large-scale motions and cannot be detected by the traditional method. With increasing x/d, the disturbance due to the apparent flapping motion of the intermedium scale grows and ultimately results in the large-scale apparent flapping motion that can be observed by the traditional method. From above, it can say that the analysis of the apparent flapping motion should also carry out in the Fourier space.

Conclusions

The following main results are summarized.

(1) The wavelet correlation analysis can extract the information of coherent strength and phase in terms of period and time delay, which is lost if the data are analyzed only by the traditional correlation method.

(2) The peaks of wavelet correlation coefficients in the high period region correspond to large peaks in $R(\tau)$, and the peaks of wavelet correlation coefficients in the low period region are equivalent to small peaks in $R(\tau)$.

(3) In branching structures of wavelet correlation coefficients or phase, the correlation peak in the high period region consists of the correlation peaks in the low period region. That is, a periodic large-scale motion contains periodic smaller scale motions.

(4) From the time between local maxima or minima or the period of peaks in wavelet cross-correlation coefficients, the convective velocities of various scales that dominate the flow structure can easily be determined.

(5) From distribution of $RWR_{xy}(a, \tau)$ at $x/d = 5$, it is found that the two-dimensionality of the periodic vortex street contains three periodic eddies and several irregular small eddies on opposite sides of the centerline.

(6) In the shear layer of $x/d = 10$, any information of auto-correlation cannot be obtained from $R(\tau)$, but the strong periodic motions of eddy for $a = 75$, 100, and 150 ms are clearly observed in wavelet auto-correlation coefficients.

(7) The large-scale motions remain symmetric and periodic in the shear layer at $x/d = 10$. From distribution of $RWR_{xy}(a, \tau)$, however, it is evident that the apparent flapping motion appears in the region of intermedium scale.

Acknowledgment

This work was performed as part of research supported by a scientific research fund granted by Japanese Ministry of Education, Science and Culture (No. 07750202).

References

Antonia, R. A., Browne, L. W., Rajagopalan, S., and Chambers, A. J., 1983, ''On the Organized Motion of a Turbulent Plane Jet,'' *Journal of Fluid Mechanics*, Vol. 134, pp. 49–66.

Argoul, F., Arneodo, A., Grasseau, G., Gagne, Y., Hopfinger, E. J., and Frisch, U., 1989, ''Wavelet Analysis of Turbulence Reveals the Multifractal Nature of the Richardson Cascade,'' *Nature*, Vol. 338, No. 2, pp. 51–53.

Bacry, E., Arneodo, A., Frisch, U., Gagne, Y. and Hopfinger, E., 1991, ''Wavelet Analysis of Fully Developed Turbulence Data and Measurement of Scaling Exponents,'' *Turbulence and Coherent Structures*, Kluwer Academic Publishers, pp. 203–215.

Benaissa A., Anselmet F., Moret-Bailly F. and Liandrat J., 1993, ''Experimental Analysis of Coherent Motions in a Turbulent Boundary Layer,'' *Eddy Structure Identification in Free Turbulent Shear Flows*, J. P. Bonnet and M. N. Glauser, eds., Kluwer Academic Publishers, pp. 159–168.

Benzi, R., and Vergassola, M., 1991, ''Optimal Wavelet Transform and its application to Two Dimensional Turbulence,'' *Fluid Dynamics Research*, Vol. 8, pp. 117–126.

Crow S. C., and Champagne, F. H., 1971, ''Orderly Structure in Jet Turbulence,'' *Journal of Fluid Mechanics*, Vol. 48, 547–591.

Dallard, T., and Browand, F. K., 1993, ''Scale Transitions at Defect Sites in the Mixing Layer: Application of the 2-D Arc Wavelet Transform,'' *Journal of Fluid Mechanics*, Vol. 247, pp. 339–368.

Dallard, T., and Spedding, G. R., 1993, ''2-D Wavelet Transform: Generalisation of the Hardy Space and Application to Experimental Studies,'' *European Journal of Mechanics B/Fluids*, Vol. 12, pp. 107–134.

Everson, R., and Sirovich, L., 1990, ''Wavelet Analysis of the Turbulent Jet,'' *Physics Letters*, Vol. 145, No. 6, pp. 314–322.

Farge, M., 1992, ''Wavelet Transforms and Their Applications to Turbulence,'' *Annual Review of Fluid Mechanics*, Vol. 24, pp. 395–457.

Farge, M., Kevlahan, N., Perrier, V., and Goirand, E., 1996, ''Wavelets and Turbulence,'' *Proceedings of the IEEE*, Vol. 84, No. 4, pp. 639–669.

Gervantes, de Gortari, J. G., and Goldschmidt, V. W., 1981, ''The Apparent Flapping Motion of a Turbulent Plane Jet—Further Experimental Results,'' ASME JOURNAL OF FLUIDS ENGINEERING, Vol. 103, No. 1, pp. 119–126.

Goldschmidt, V. W., and Bradshaw, P., 1973, ''Flapping of a Plane Jet,'' *Physics of Fluids*, Vol. 16, pp. 354–355.

Goldshmidt, V. W., Young, M. F., and Ott, E. S., 1981, ''Turbulent Convective Velocities (Broadband and Wavenumber Dependent) in a Plane Jet,'' *Journal of Fluid Mechanics*, Vol. 105, pp. 327–345.

Gordeyev, S. V., and Thomas, F. O., 1995, ''Measurement of Reynolds Stress Reversal in a Planar Jet by Means of a Wavelet Decomposition,'' *Turbulent Flows*, ASME, FED-Vol. 208, pp. 49–54.

Gordeyev, S. V., Thomas F. O., and Chu, H. C., 1995, ''Experimental Investigation of Unsteady Jet Shear Layer Dynamics Using a Wavelet Decomposition,'' *Unsteady Flows*, ASME, FED-Vol. 216, pp. 167–172.

Goupillaud, P., Grossmann, A., and Morlet, J., 1984, ''Cycle-Octave and Related Transforms in Seismic Signal Analysis,'' *Geoexploration*, Vol. 23, pp. 85–102.

Grossmann, A., and Morlet, J., 1984, ''Decomposition of Hardy Functions ito Square Integrable Wavelets of Constant Shape,'' *SIAM J. Math. Anal.*, Vol. 15, pp. 723–736.

Gutmark, E., 1976, ''The Planar Turbulent Jet,'' *Journal of Fluid Mechanics*, Vol. 73, Part 3, pp. 465–495.

Harr, A., 1910, ''Zur Theorie der Orthogonalen Funktionen-Systeme,'' *Mathematische Annalen*, Vol. 69, pp. 331–371.

Higuchi, H., Lewalle J., and Crane P., 1994, ''On the Structure of a Two-Dimension Wake Behind a Pair of Flat Plates,'' *Physics Fluids*, Vol. 6, No. 1, pp. 297–305.

Hsiao, F. B., and Huang, J. M., 1994, ''On the Dynamics of Flow Structure Development in an Excited Plane Jet,'' ASME JOURNAL OF FLUIDS ENGINEERING, Vol. 116, No. 4, pp. 714–720.

Kaspersen, J. H., 1996, ''A Study of Coherent Structures Using Wavelet Analysis,'' Ph.D. thesis.

Krothapalli, A., Baganoff, D., and Karamcheti, K., 1981, ''On the Mixing of a Rectangular Jet,'' *Journal of Fluid Mechanics*, Vol. 107, pp. 201–220.

Lewalle, J., Petagna P. and Buresti G., 1994, ''Wavelet Statistics of the Near-Field Structure of a Coaxial Jet,'' AIAA Paper 94-2323.

Liandrat, J., and Moret-Bailly, F., 1990, ''The Wavelet Transform: Some Applications to Fluid Dynamics and Turbulence,'' *European Journal of Mechanics B/Fluids*, Vol. 9, No. 1, pp. 1–19.

Li H., 1997a, ''Wavelet Analysis on Coherent Structure Dynamics in a Plane Turbulent Jet,'' *Experimental Heat Transfer, Fluid Mechanics and Thermodynamics 1997*, Edizioni ETS, PISA, pp. 1175–1782.

Li H., 1997b, ''Wavelet Reynolds Stress Analysis of Two-Dimensional Vortex Flow,'' ASME FEDSM 97-3040.

Li, H., 1997c, ''Wavelet Velocity Correlation Analysis in a Plane Turbulent Jet,'' *Proceedings of the 11th Symposium on Turbulent Shear Flows*, Vol. 3, P3-101–106.

Li, H., 1997d, ''Turbulent Structure Analysis of a Two-Dimensional Jet Using Wavelets,'' *Proceedings of the 5th Triennial International Symposium on Fluid Control, Measurement and Visualization*, pp. 589–594.

Li, H., and Nozaki, T., 1995, ''Wavelet Analysis for the Plane Turbulent Jet (Analysis of Large Eddy Structure),'' *JSME International Journal, Fluids and Thermal Engineering*, Vol. 38, No. 4, pp. 525–531.

Li, H., Nozaki, T., Tabata T., and Oshige S., 1997, ''Wavelet Analysis of Flow Structure in a Bounded Jet,'' *Proceedings of International Conference on Fluid Engineering*, Vol. 2, No. 97-107, pp. 589–594.

Li, H., Takei, M., Ochi, M., Saito, Y., and Horii, K., 1998a, ''Velocity Correlation Analysis in the Near-Field of a Turbulent Jet With Help of Discrete Wavelet Transform,'' ASME FEDSM98-4823.

Li, H., Takei, M., Ochi, M., Saito, Y., and Horii, K., 1998b, ''Multiresolution Visualization of the Turbulent Jet,'' *Album of Visualization*, No. 15, pp. 11–12.

Li, H., Takei, M., Ochi, M., Saito, Y., and Horii, K., 1998c, ''Effect of Different Orthogonal Wavelet Basis on Multiresolution Image Analysis of a Turbulent Flow,'' *CD-ROM Proceedngs of International Conference on Optical Technology and Image.*

Li, H., and Tomita, Y., 1997, ''Wavelet Statistical Analysis of Gas-Solid Flow in a Vertical Pipeline,'' *Experimental Heat Transfer, Fluid Mechanics and Thermodynamics 1997*, Edizioni ETS, PISA, pp. 1053–1060.

Li, H., and Tomita, Y., 1998, ''Wavelet Analysis of Gas-Solid Two-Phase Flow in a Horizontal Pipe,'' *CD-ROM Proceedings of Third International Conference on Multiphase Flow.*

Morlet, J., Arens, G., Fourgeau, I., and Giard D., 1982, ''Wave Propagation and Sampling Theory,'' *Geophysics*, Vol. 47, pp. 203–236.

Moum, J. N., Kawall, J. G., and Keffer, J. F., 1979, ''Structure Features of the Plane Turbulent Jet,'' *Physics Fluids*, Vol. 22, No. 7, pp. 1240–1249.

Mumford, J. C., 1982, ''The Structure of the Large Eddies in Fully Developed Turbulent Shear Flows. Part 1. The Plane Jet,'' *Journal of Fluid Mechanics*, Vol. 118, pp. 241–268.

Oler, J. W., and Goldschmidt, V. W., 1984, ''Coherent Structures in the Similarity Region of Two-Dimensional Turbulent Jets,'' ASME JOURNAL OF FLUIDS ENGINEERING, Vol. 106, No. 2, pp. 187–192.

Quinn, W. R., 1994, ''Development of a Large-Aspect-Ratio Rectangular Turbulent Free Jet,'' *AIAA Journal*, Vol. 32, No. 3, pp. 547–554.

Spedding, G. R., Browand, F. K., Huang N. E., and Long S. R., 1993, ''A 2-D Complex Wavelet Analysis of an Unsteady Wind-Generated Surface Wave Field,'' *Dynamics of Atmospheres and Oceans*, Vol. 20, pp. 55–77.

Sullivan, P., and Pollard, A., 1996, ''Coherent Structure Identification from the Analysis of Hot-Wire Data,'' *Measurement of Science Technology*, Vol. 7, pp. 1498–1516.

Thomas, F. O., and Chu, H. C., 1993, ''Nonlinear Wave Coupling and Subharmonic Resonance in Planar Jet Shear Layer Transition,'' *Physics Fluids A*, Vol. 5, No. 3, pp. 630–646.

Walker, S. H., Gordeyev, S. V., and Thomas, F. O., 1995, ''A Wavelet Transform Analysis Applied to Unsteady Jet Screech Resonance,'' *High Speed Jet Flows ASME*, FED-Vol. 214, pp. 103–108.

Weierstrass, K., 1895, ''Mathematische Werke,'' Vol. 2, Mayer & Muller, Berlin.

Yamada, M. and Ohkitani, K., 1990, ''Orthonormal Wavelet Expansion and Its Application to Turbulence,'' *Progress of Theoretical Physics*, Vol. 83, No. 5, pp. 819–823.

Yoda, M., Hesselink, L., and Mungal, M. G., 1992, ''The Evolution and Nature of Large-Scale Structures in the Turbulent Jet,'' *Physics Fluids A*, Vol. 4, No. 4, pp. 803–811.

Yule, A. J., 1978, ''Large-scale Structure in the Mixing Layer of a Round Jet,'' *Journal of Fluid Mechanics*, Vol. 89, pp. 413–432.